

MIT Open Access Articles

*A Third Exoplanetary System with
Misaligned Orbital and Stellar Spin Axes*

The MIT Faculty has made this article openly available. **Please share**
how this access benefits you. Your story matters.

Citation: Johnson, John Asher et al. "A Third Exoplanetary System with Misaligned Orbital and Stellar Spin Axes1." Publications of the Astronomical Society of the Pacific 121.884 (2009): 1104–1111. Web. DOI:10.1086/644604.

Publisher: University of Chicago Press

Persistent URL: <http://hdl.handle.net/1721.1/77088>

Version: Author's final manuscript: final author's manuscript post peer review, without publisher's formatting or copy editing

Terms of use: Creative Commons Attribution-Noncommercial-Share Alike 3.0



A THIRD EXOPLANETARY SYSTEM WITH MISALIGNED ORBITAL AND STELLAR SPIN AXES¹

JOHN ASHER JOHNSON^{2,3}, JOSHUA N. WINN⁴, SIMON ALBRECHT⁴,
 ANDREW W. HOWARD^{5,6}, GEOFFREY W. MARCY⁵, J. ZACHARY GAZAK²

Draft version July 30, 2009

ABSTRACT

We present evidence that the WASP-14 exoplanetary system has misaligned orbital and stellar-rotational axes, with an angle $\lambda = -33.1^\circ \pm 7.4^\circ$ between their sky projections. The evidence is based on spectroscopic observations of the Rossiter-McLaughlin effect as well as new photometric observations. WASP-14 is now the third system known to have a significant spin-orbit misalignment, and all three systems have “super-Jupiter” planets ($M_P > 3 M_{\text{Jup}}$) and eccentric orbits. This finding suggests that the migration and subsequent orbital evolution of massive, eccentric exoplanets is somehow different from that of less massive close-in Jupiters, the majority of which have well-aligned orbits.

Subject headings: stars: individual (WASP-14)—planetary systems: individual (WASP-14b)—techniques: spectroscopic—techniques: photometric

1. INTRODUCTION

Close-in giant planets are thought to have formed at distances of several AU and then migrated inward to their current locations (Lin et al. 1996). The mechanism responsible for the inward migration of exoplanets is still debated. Some clues about the migration process may come from constraints on the stellar obliquity: the angle between the stellar spin axis and the orbital axis. The sky projection of this angle, λ , can be measured by observing and interpreting the anomalous Doppler shift during the transit of a planet, known as the Rossiter-McLaughlin effect (McLaughlin 1924; Rossiter 1924; Queloz et al. 2000; Winn et al. 2005; Ohta et al. 2005; Gaudi & Winn 2007). Some of the proposed migration pathways would produce large misalignments (at least occasionally) while others would preserve the presumably close alignment that characterizes the initial condition of planet formation.

For example, theories that invoke migration of the planet through interactions with the gaseous protoplanetary disk predict small spin-orbit angles, and that initial spin-orbit misalignments and eccentricities should be damped out (Lin et al. 1996; Moorhead & Adams 2008; Lubow & Ogilvie 2001). On the other hand, impulsive processes such as close encounters between planets (Chatterjee et al. 2008; Ford & Rasio 2008) or dynamical relaxation (Jurić & Tremaine 2008) should drive systems out of alignment. The Kozai mechanism also pro-

duces large orbital tilts (Wu & Murray 2003, Fabrycky & Tremaine 2007). Ultimately the hope is that the predictions of migration theories can be compared with an ensemble of measurements of λ (Fabrycky & Winn 2009).

In this paper we add the transiting exoplanet WASP-14b to the growing collection of systems for which the projected spin-orbit angle has been measured. WASP-14 is a relatively bright ($V = 9.75$) F5V star which was discovered by the Wide-Angle Search for Planets (Super-WASP) to undergo periodic transits by a Jovian planet every 2.2 days (Joshi et al. 2009, hereafter J09). The planet is among the most massive of the known transiting exoplanets, with $M_P = 7.3 M_{\text{Jup}}$, and it has a measurably eccentric orbit ($e = 0.090 \pm 0.003$), which is unusual among the hot Jupiters. J09 also reported a measurement of the spin-orbit angle, $\lambda = -14^{+21}_{-14}$ degrees, which is consistent with zero, but also allows for the possibility of a significant misalignment. In the following section we describe our spectroscopic and photometric observations of WASP-14, made in an attempt to refine the measurement of λ . In § 3 we present evidence for a large spin-orbit misalignment based on our radial-velocity measurements obtained during transit. We summarize the results of our joint analysis of our photometric and spectroscopic monitoring in § 4, and present tentative evidence of an emerging trend between spin-orbit misalignment, and the physical and orbital characteristics of close-in exoplanets.

2. OBSERVATIONS AND DATA REDUCTION

2.1. Radial Velocity Measurements

We observed the transit predicted by J09 to occur on 2009 June 17 using the High-Dispersion Spectrometer (HDS, Noguchi et al. 2002) on the Subaru 8.2m Telescope atop Mauna Kea in Hawaii. We obtained spectra of WASP-14 through an iodine cell using the I2b spectrometer setting and a 0.8 slit, providing a resolution of approximately 60,000. We started our observing sequence just after evening twilight, about 20 min before the predicted time of ingress. We continued our observations until 2.5 hr after egress when the star set below 20° elevation. For most of our observations we used exposure times of 5 min, yielding a signal-to-noise ratio (SNR) of

Electronic address: johnjohn@ifa.hawaii.edu

¹ Based on data collected at Subaru Telescope, which is operated by the National Astronomical Observatory of Japan; the Keck Observatory, which is operated as a scientific partnership among the California Institute of Technology, the University of California, and the National Aeronautics and Space Administration; and the UH 2.2-meter telescope.

² Institute for Astronomy, University of Hawaii, Honolulu, HI 96822; NSF Astronomy and Astrophysics Postdoctoral Fellow

³ NSF Astronomy and Astrophysics Postdoctoral Fellow

⁴ Department of Physics, and Kavli Institute for Astrophysics and Space Research, Massachusetts Institute of Technology, Cambridge, MA 02139

⁵ Department of Astronomy, University of California, Mail Code 3411, Berkeley, CA 94720

⁶ Townes Postdoctoral Fellow, Space Sciences Laboratory, University of California, Berkeley, CA 94720-7450 USA

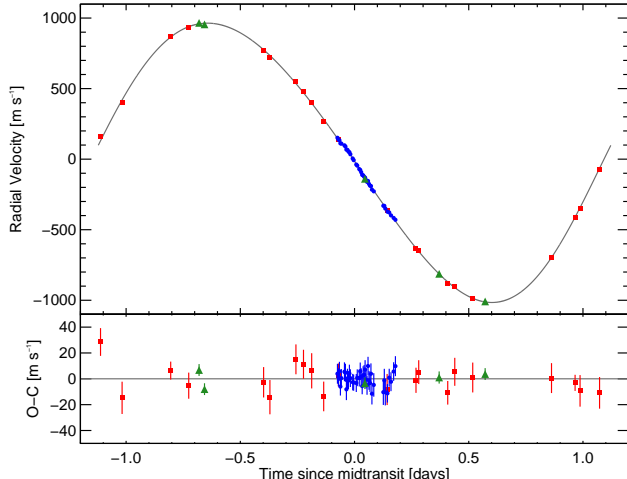


FIG. 1.— Relative radial velocity measurements of WASP-14 as a function of orbital phase, expressed in days since midtransit. The symbols are as follows: Subaru (circles), Keck (squares), Joshi et al. 2009 (triangles). The lower panel shows the residuals after subtracting the best-fitting model including both the Keplerian radial velocity and the Rossiter-McLaughlin effect.

100–120 pixel^{−1} at 5500 Å, the central wavelength of the range with plentiful iodine absorption lines. At high air-mass we increased our exposure times to 10 min.

We also obtained 8 radial velocity measurements of the G2V star HD 127334 on the same night, 2009 June 17. HD 127334 is a long-term target of the California Planet Search. Keck/HIRES radial velocity measurements over the past 3 years show that the star is stable with an rms scatter of 2.5 m s^{−1}. With HDS we used exposure times ranging from 60 to 120 seconds, resulting in SNR ranging from 110–120 pixel^{−1} at 5500 Å.

We also obtained out-of-transit (OOT) radial velocities of WASP-14 using the High-Resolution (HIRES) spectrometer on the Keck I telescope starting in July 2008. We set up the HIRES spectrometer in the same manner that has been used consistently for the California Planet Search (Howard et al. 2009). Specifically, we employed the red cross-disperser and used the I₂ absorption cell to calibrate the instrumental response and the wavelength scale (Marcy & Butler 1992). The slit width was set by the 0′.86 B5 decker, and the typical exposure times ranged from 3–10 min, giving a resolution of about 60,000 and a SNR of 140–250 pixel^{−1} at 5500 Å.

For the spectra obtained at both telescopes, we performed the Doppler analysis with the algorithm of Butler et al. (1996), as updated over the years. A clear, Pyrex cell containing iodine gas is placed in front of the spectrometer entrance slit. The dense forest of molecular lines imprinted on each stellar spectrum provides a measure of the wavelength scale at the time of the observation, as well as the shape of the instrumental response (Marcy & Butler 1992). The Doppler shifts were measured with respect to a “template” spectrum based on a higher-resolution Keck/HIRES observation from which the spectrometer instrumental response was removed, as far as possible, through deconvolution. We estimated the measurement error in the Doppler shift derived from a given spectrum based on the weighted standard deviation of the mean among the solutions for individual 2 Å spectral segments. The typical measurement error was

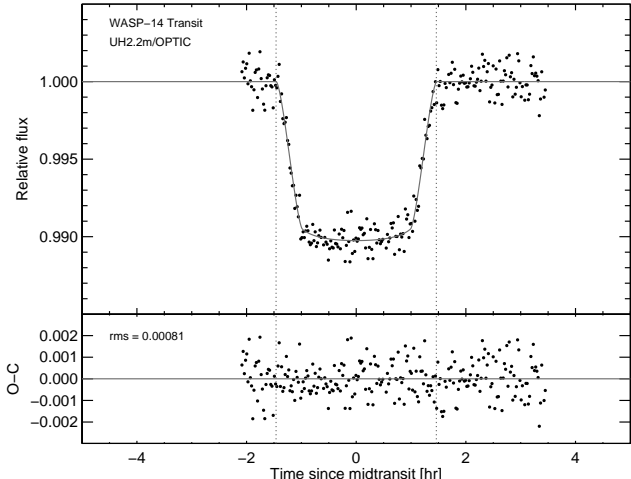


FIG. 2.— *Top Panel:* Relative photometry of WASP-14 during the transit of 2009 May 12. *Bottom Panel:* Residuals from the best-fitting transit light curve model.

1.0–1.7 m s^{−1} for the Keck data and 6 m s^{−1} for the Subaru data. The RV data are given in Table 1 and plotted in Figure 1.

2.2. Photometric Measurements

We observed the photometric transit of 2009 May 12 with the University of Hawaii 2.2 m (UH2.2m) telescope on Mauna Kea. We used the Orthogonal Parallel Transfer Imaging Camera (OPTIC), which is equipped with two Lincoln Labs CCID128 orthogonal transfer array (OTA) detectors (Tonry et al. 1997). Each OTA detector has 2048×4096 pixels and a scale of 0′.135 pixel^{−1}. OTA devices can shift accumulated charge in two dimensions during an exposure. We took advantage of this charge-shifting capability to create large square-shaped point spread functions (PSFs) that permit longer exposures before reaching saturation (Howell et al. 2003; Tonry et al. 2005; Johnson et al. 2009).

We observed the transit of WASP-14 continuously for 5.5 hr spanning the transit. We observed through a custom bandpass filter centered at 850 nm with a 40 nm full-width at half-maximum. We shifted the accumulated charge every 50 ms to trace out a square-shaped region 25 pixels on a side. Exposure times were 50 s, and were separated by a gap of 29 s to allow for readout and refreshing of the detectors. Bias subtraction and flat-field calibrations were applied using custom IDL procedures described by Johnson et al. (2009).

The only suitable comparison star that fell within the OPTIC field of view is a $V = 12.1$ star ~ 6 arcminutes to the Northeast. The fluxes from the target and the single comparison star were measured by summing the counts within a square aperture of 64 pixels on a side. Most of the light, including the scattered-light halo, was encompassed by the aperture. We estimated the background from the outlier-rejected mean of the counts from four rectangular regions flanking each of the stars (Johnson et al. 2009). As a first order correction for variations in sky transparency, we divided the the flux of WASP-14 by the flux of the comparison star. The transit light curve is shown in Figure 2, and the photometric measurements and times of observations (HJD) are listed

in Table 2.

3. DATA ANALYSIS

3.1. Updated Ephemeris

The first step in our analysis was to refine the estimate of the orbital period using the midtransit time derived from our OPTIC light curve. We fitted a transit model to the light curve based on the analytic formulas of Mandel & Agol (2002) for a quadratic limb-darkening law. The adjustable parameters were the midtransit time T_t , the scaled stellar radius R_\star/a (where a is the semimajor axis), the planet-star radius ratio R_p/R_\star , the orbital inclination i , the limb darkening coefficients u_1 and u_2 ⁷, and two parameters k and m_0 describing the correction for differential airmass extinction. The airmass correction was given by

$$m_{\text{cor}} = m_{\text{obs}} + m_0 + kz \quad (1)$$

where m_{obs} is the observed instrumental magnitude, z is the airmass, and m_{cor} is the corrected magnitude that is compared to the transit model (Winn et al. 2009).

We used the rms of the OOT measurements as an estimate for the individual measurement uncertainties. We did not find evidence for significant time-correlated noise using the time-averaging method of Pont et al. (2006). We fitted the light curve model and estimated our parameter uncertainties using a Markov Chain Monte Carlo algorithm (MCMC; Tegmark et al. 2004; Ford 2005; Gregory 2005). The results for the midtransit time, and the refined orbital period (using the new midtransit time and the midtransit time given by J09) are

$$T_c = 2454889.8921 \pm 0.00025 \quad (2)$$

$$P = 2.2437704 \pm 0.0000028 \text{ days.} \quad (3)$$

The other derived lightcurve parameters were consistent with those reported by J09.

3.2. Evidence for Spin-Orbit Misalignment: A Simple Analysis

Figure 2 shows our Subaru/HDS and Keck/HIRES RV measurements made near transit, after subtracting the best-fitting Keplerian orbital model. The RVs measured just after ingress are redshifted with respect to the Keplerian orbital velocity. We interpret this “anomalous” redshift as being due to the blockage by the planet of the blueshifted limb of the rotating stellar surface. We therefore conclude that the planet’s orbit is prograde.

In addition, the anomalous redshift persists until about 1 hr after midtransit. This is evidence for a misalignment between the orbital axis and stellar rotation axis. Were $\lambda = 0$, the midpoint of the transit chord would be on the projection of the stellar rotation axis, and therefore the anomalous Doppler shift would vanish at midtransit, in contradiction of the data. Thus we can conclude that the orbit of WASP-14b is inclined with respect to the projected stellar spin axis. In the next section we make a quantitative assessment of λ .

⁷ We allowed both coefficients to be free parameters, subject to the conditions $0 < u_1 + u_2 < 1$ and $u_1 > 0$.

3.3. Global Analysis of Radial Velocities and Photometry

We simultaneously fitted a parametric model to our OPTIC light curve and to the 4 sets of RV data: Subaru/HDS and Keck/HIRES (this work), and OHP/SOPHIE and NOT/FIES (J09). To make our analysis of the RM effect largely independent of J09, we did not include the RVs gathered by J09 during transits. The photometric aspects of the model were given in § 3.1. The RV model was the sum of the radial component of the Keplerian orbital velocity, and the anomalous velocity due to the Rossiter-McLaughlin effect. To compute the latter, we used the “RM calibration” procedure of Winn et al. (2005): we simulated spectra exhibiting the RM effect at various orbital phases⁸, and then measured the anomalous radial velocity ΔV_R of the simulated spectra using the same algorithm used on the actual data. We found the results to be consistent with the formula

$$\Delta V_R = -(\delta f)v_p \left[1.124 - 0.395 \left(\frac{v_p}{3.5 \text{ km s}^{-1}} \right)^2 \right], \quad (4)$$

where δf is the instantaneous fractional loss of light during the transit and v_p is the radial velocity of the occulted portion of the stellar disk.

The 18 model parameters can be divided into 3 groups. First are the parameters of the spectroscopic orbit: the period P , the midtransit time T_t , the radial-velocity semiamplitude K , the eccentricity e , the argument of pericenter ω , and velocity offsets for each of the 4 different groups of RV data. Second are the photometric parameters: the planet-to-star radius ratio R_p/R_\star , the orbital inclination i , the scaled stellar radius R_\star/a (where a is the semimajor axis), the 2 limb-darkening coefficients, and the out-of-transit flux and differential extinction coefficient. Third are the parameters relevant to the RM effect: the projected stellar rotation rate $v \sin i_\star$ and the angle λ between the sky projections of the orbital axis and the stellar rotation axis [for illustrations of the geometry, see Ohta et al. (2005), Gaudi & Winn (2007), or Fabrycky & Winn (2009)].

The fitting statistic was

$$\begin{aligned} \chi^2 = & \sum_{j=1}^{247} \left[\frac{f_j(\text{obs}) - f_j(\text{calc})}{\sigma_{f,j}} \right]^2 \\ & + \sum_{j=1}^{64} \left[\frac{v_j(\text{obs}) - v_j(\text{calc})}{\sigma_{v,j}} \right]^2 \\ & + \left[\frac{P - 2.243770 \text{ d}}{0.0000028 \text{ d}} \right]^2, \end{aligned}$$

where $f_j(\text{obs})$ are the relative flux data from the OPTIC light curve and $\sigma_{f,j}$ is the out-of-transit rms. Likewise $v_j(\text{obs})$ and $\sigma_{v,j}$ are the RV measurements and uncertainties. For $\sigma_{v,j}$ we used the quadrature sum of the measurement error and a “jitter” term of 4.4 m s^{-1} , which was taken from the empirical calibration of Wright (2004).

⁸ For the template spectrum, which should be similar to that of WASP-14 but with slower rotation, we used a Keck/HIRES spectrum of HD 3681 ($T_{\text{eff}} = 6220 \text{ K}$, $[\text{Fe}/\text{H}] = +0.08$; $v \sin i_\star = 2.8 \pm 0.5 \text{ km s}^{-1}$ Valenti & Fischer 2005).

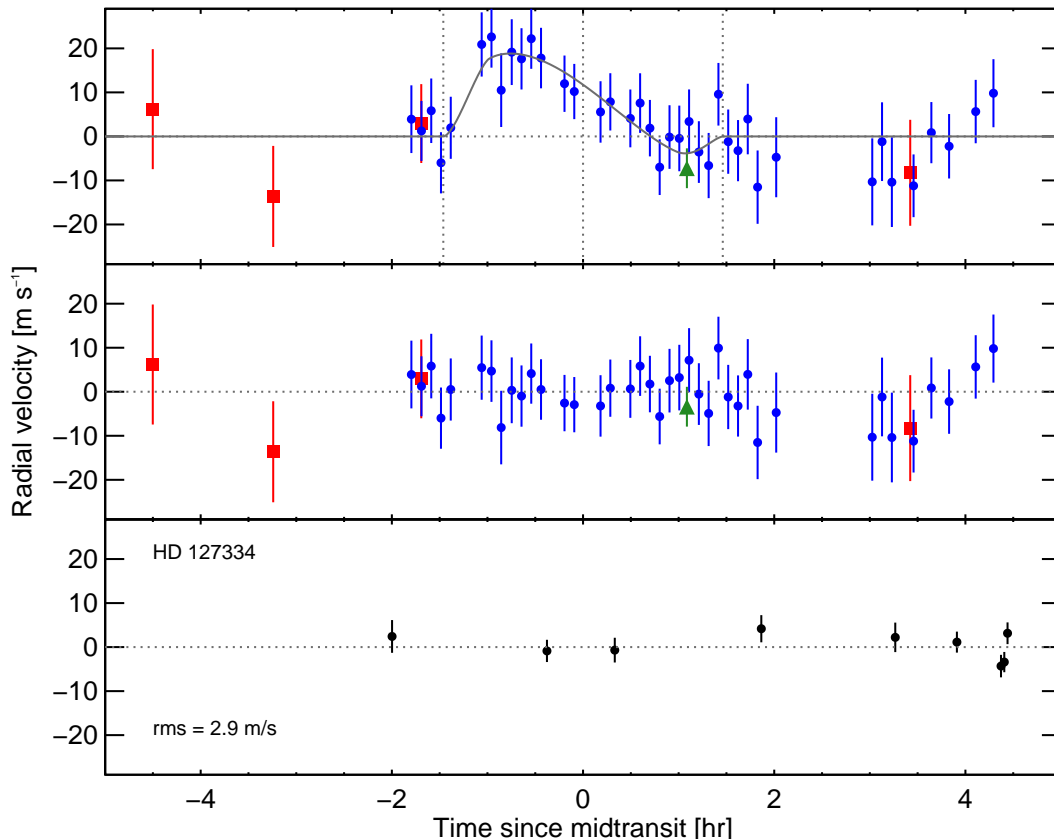


FIG. 3.— Relative radial velocity measurements made during transits of WASP-14. The symbols are as follows: Subaru (circles), Keck (squares), Joshi et al. 2009 (triangles). *Top Panel:* The Keplerian radial velocity has been subtracted, to isolate the Rossiter-McLaughlin effect. The predicted times of ingress, midtransit and egress are indicated by vertical dotted lines. *Middle Panel:* The residuals after subtracting the best-fitting model including both the Keplerian radial velocity and the RM effect. *Bottom Panel:* Subaru/HDS measurements of the standard star HD 127334 made on the same night as the WASP-14 transit.

The final term enforces the constraint on the orbital period based on the new ephemeris described in the previous section.

As before, we solved for the model parameters and uncertainties using a Markov Chain Monte Carlo algorithm. We used a chain length of 5×10^6 steps and adjusted the perturbation size to yield an acceptance rate of $\sim 40\%$. The posterior probability distributions for each parameter were approximately Gaussian, so we adopt the median as the “best-fit” value and the standard deviation as the $1\text{-}\sigma$ error. For the joint model fit the minimum χ^2 is 291.4 with 295 degrees of freedom, giving $\chi^2_\nu = 0.99$. The contributions to the minimum χ^2 from the flux data and the RV data were 246.1 and 45.3, respectively. The relatively low value of the RV contribution compared to the number of RV data points (64) suggests that 4.4 m s^{-1} is an overestimate of the jitter for this star, and that consequently our parameter errors may be slightly overestimated, but to be conservative we give the results assuming a jitter of 4.4 m s^{-1} .

For the main parameter of interest, the projected spin-orbit angle, our analysis gives $\lambda = 1 \pm 7.4^\circ$ (Figure 3). Thus, the WASP-14 planetary system is prograde and misaligned, as anticipated in the qualitative discussion of § 3.2. Our measurement of λ agrees with the value measured by J09 (-14^{+21}_{-14} deg), but with improved precision that allows us to exclude $\lambda = 0$ with high confidence.

We find the projected stellar rotational velocity to be $v \sin i_\star = 2.80 \pm 0.57 \text{ km s}^{-1}$. This value is somewhat lower than, but consistent with, the values determined by J09 from line broadening $v \sin i_\star = 3.0 \pm 1.5 \text{ km s}^{-1}$, from their RM analysis $v \sin i_\star = 4.7 \pm 1.5 \text{ km s}^{-1}$, and from our SME analysis $v \sin i_\star = 3.5 \pm 0.5 \text{ km s}^{-1}$. This agreement among the rotation rates provides a consistency check on our analysis. The best-fitting parameters and their uncertainties are listed in Table 3

We found no evidence for another planet or star in the WASP-14 system. To derive quantitative constraints on the properties of any distant planets, we added a single new parameter $\dot{\gamma}$ to our model, representing a constant radial acceleration. A third body with mass $M_3 \ll M_\star$, orbital distance $a_3 \gg a$ and inclination i_3 would produce a typical radial acceleration

$$\dot{\gamma} \sim \frac{GM_3 \sin i_3}{a_3^2}, \quad (5)$$

and our result is $\dot{\gamma} = 2.0 \pm 1.4 \text{ cm s}^{-1} \text{ d}^{-1}$, or $1.01 \pm 0.72 M_{\text{Jup}} (5 \text{ AU})^{-2}$.

4. SUMMARY AND DISCUSSION

We present new photometric and spectroscopic measurements of the WASP-14 transiting exoplanetary system. By combining a new transit light curve, several Keck/HIRES RV measurements made outside of transit, and most importantly, Subaru/HDS RVs spanning a

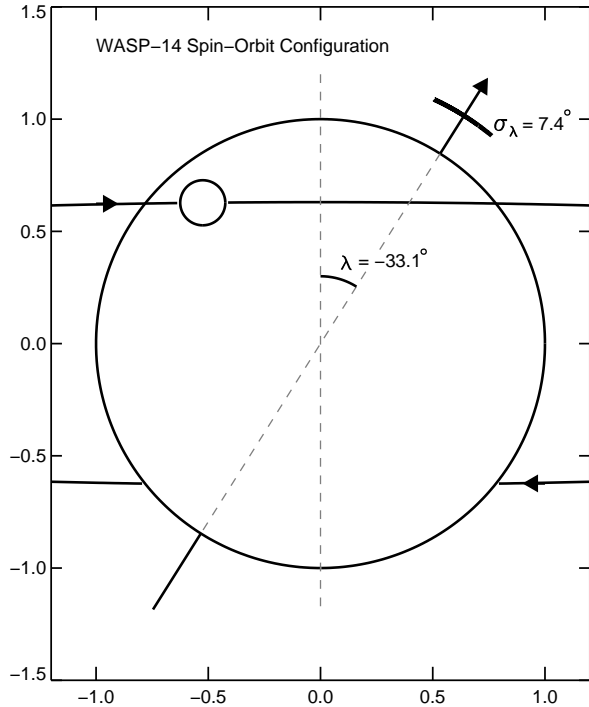


FIG. 4.— The spin-orbit configuration of the WASP-14 planetary system. The star has a unit radius and the relative size of the planet and impact parameter are taken from the best-fitting transit model. The sky-projected angle between the stellar spin axis (diagonal dashed line) and the planet’s orbit normal (vertical dashed line) is denoted by λ , which in this diagram is measured counter-clockwise from the orbit normal. Our best-fitting λ is negative. The 68.3% confidence interval for λ is traced on either side of the stellar spin axis and denoted by σ_λ .

transit, we have measured and interpreted the RM effect. By modeling the RM anomaly we find that the projected stellar spin axis and the planetary orbit normal are misaligned, with $\lambda = -33.1^\circ \pm 7.4^\circ$.

Of the 13 transiting systems with measured spin-orbit angles, only 3 have clear indications of spin-orbit misalignments. The other two cases besides WASP-14 are XO-3 (Hébrard et al. 2008, Winn et al. 2009) and HD 80606 (Gillon 2009; Pont et al. 2009; Winn et al. 2009c in prep). It is striking that all 3 tilted systems involve planets several times more massive than Jupiter that are on eccentric orbits, and that none of the systems with eccentricities consistent with circular or with masses smaller than $1 M_{\text{Jup}}$ show evidence for misalignments (Figure 5).

In addition to the three known super-Jupiters with inclined orbits, there are also two eccentric, massive exoplanets with small projected spin-orbit angles: HD 17156 b (Fischer et al. 2007; Barbieri et al. 2007; Cochran et al. 2008; Narita et al. 2009) and HD 147506 (Bakos et al. 2007; Winn et al. 2007; Loeillet et al. 2008). However, neither of these cases presents as strong an exception to the pattern as it may seem. The measurement of λ in both cases was hampered by the poor constraint on the transit impact parameter, which causes a strong degeneracy between λ and $v \sin i$ (Gaudi & Winn 2007). It should also be kept in mind that the measured quantity λ is only the *sky-projected* spin-orbit

angle, and that the true angle of one or both of those systems may have a stellar rotation axis that is inclined by a larger angle along our line of sight.

It was already known that the orbits of massive planets are systematically different from the orbits of less massive planets. For example, Wright et al. (2009), building on a previous finding by Marcy et al. (2005), showed that planets with minimum masses $M_P \sin i > 1 M_{\text{Jup}}$ typically have lower orbital eccentricities than those with minimum masses smaller than $1 M_{\text{Jup}}$. While sub-Jovian-mass planets have eccentricities that peak near $e = 0$ with a sharp decline toward $e = 0.4$, those with $M_P \sin i > 1 M_{\text{Jup}}$ have eccentricities that are uniformly distributed between $e = 0$ and 0.55.

The tendency for misaligned orbits to be found among massive planets on eccentric orbits does not yet have a clear interpretation. It may seem natural for inclined orbits and eccentric orbits to go together, since both inclinations and eccentricities can be excited by few-body dynamical interactions, whether through the Kozai effect, (Fabrycky & Tremaine 2007; Wu et al. 2007) planet-planet scattering (Jurić & Tremaine 2008, see, e.g.), or scenarios combining both of these phenomena (Nagasawa et al. 2008). However, the mass dependence of these and other mechanisms for altering planetary orbits needs to be clarified before any comparisons can be made to the data.

The misalignment of the WASP-14 planetary system, along with the previously discovered misaligned systems, have offered a tantalizing hint of an emerging trend among the orbital and physical properties of close-in, transiting exoplanets. However, trends seen in small data sets can often be misleading. To bring this picture into better focus, a more sophisticated analysis of the extant data, following the example of Fabrycky & Winn (2009) may be better. And as with all astrophysical trends, observations of a larger sample of objects will provide a much clearer picture than any statistical analysis of a smaller sample. Thus, additional RM observations of transiting systems are warranted, with particular attention paid to trends with orbital eccentricity and planet mass.

We thank the referee, Dan Fabrycky, for a remarkably timely and helpful review. We gratefully acknowledge the assistance of the UH 2.2 m telescope staff, including Edwin Sousa, Greg Osterman and John Dvorak. Special thanks to John Tonry for his helpful discussions and comprehensive instrument documentation for OPTIC, Debra Fischer for her HDS raw reduction code, and Scott Tremaine for his helpful comments and suggestions. JAJ is an NSF Astronomy and Astrophysics Postdoctoral Fellow with support from the NSF grant AST-0702821. JNW thanks the NASA Origins of Solar Systems program for support through awards NNX09AD36G and NNX09AB33G, as well as the support of the MIT Class of 1942 Career Development Professorship. SA acknowledges support by a Rubicon fellowship from the Netherlands Organisation for Scientific Research (NWO). We also appreciate funding from NASA grant NNG05GK92G (to GWM), and AWH gratefully acknowledges support from a Townes Postdoctoral Fellowship at the UC Berkeley Space Sciences Lab-

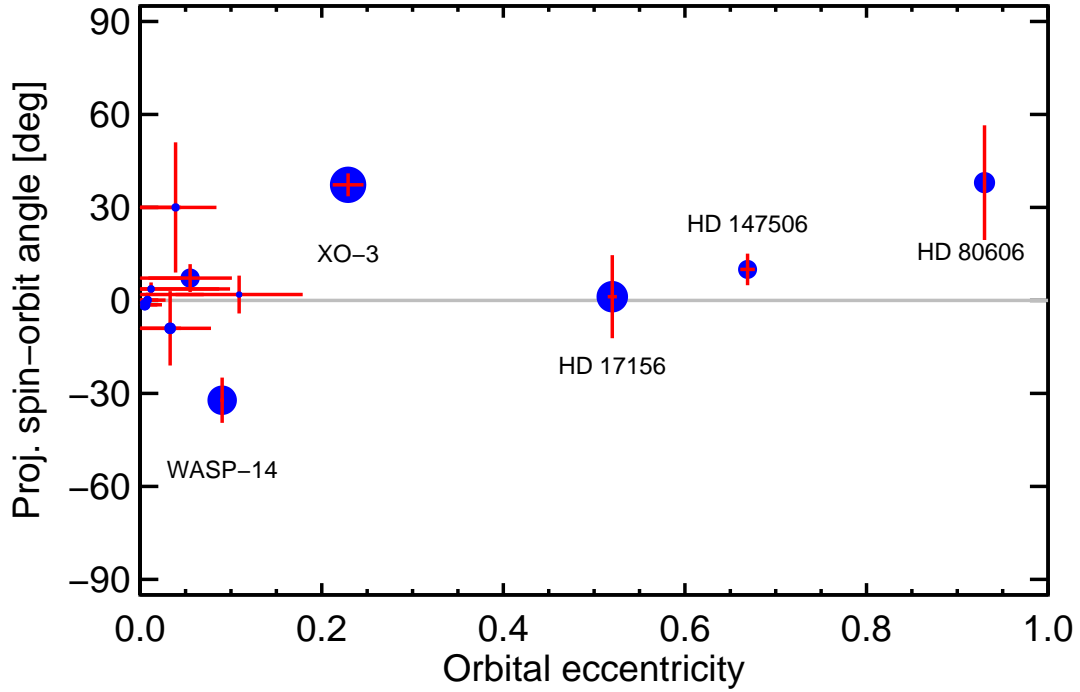


FIG. 5.— The eccentricities and projected spin-orbit angles for the 13 transiting systems for which the Rossiter-McLaughlin effect has been observed and modeled. The data are from Table 1 of Fabrycky & Winn (2009) and Madhusudhan & Winn (2008) as updated by Winn et al. (2009), Narita et al. (2009) and this work. The size of the plot symbols scales as $M_P^{1/2}$, and the error bars show the measurement uncertainties for both eccentricity and the spin-orbit angle. For the systems consistent with $e = 0$ the horizontal error bar gives the 95.4% confidence upper limit on e , and for the other systems the horizontal error bars represent the 68.3% confidence uncertainties.

oratory. The authors wish to extend special thanks to those of Hawaiian ancestry on whose sacred mountain of Mauna Kea we are privileged to be guests. Without their

generous hospitality, the observations presented herein would not have been possible.

REFERENCES

- Bakos, G. Á., et al. 2007, *ApJ*, 670, 826
 Barbieri, M., et al. 2007, *A&A*, 476, L13
 Butler, R. P., et al. 1996, *PASP*, 108, 500
 Chatterjee, S., Ford, E. B., Matsumura, S., & Rasio, F. A. 2008, *ApJ*, 686, 580
 Cochran, W. D., Redfield, S., Endl, M., & Cochran, A. L. 2008, *ApJ*, 683, L59
 Fabrycky, D. & Tremaine, S. 2007, *ApJ*, 669, 1298
 Fabrycky, D. C. & Winn, J. N. 2009, *arxiv:0902.0737*
 Fischer, D. A., et al. 2007, *ApJ*, 669, 1336
 Ford, E. B. 2005, *AJ*, 129, 1706
 Ford, E. B. & Rasio, F. A. 2008, *ApJ*, 686, 621
 Gaudi, B. S. & Winn, J. N. 2007, *ApJ*, 655, 550
 Gillon, M. 2009, *ArXiv e-prints*
 Gregory, P. C. 2005, *ApJ*, 631, 1198
 Howard, A. W., et al. 2009, *arxiv:0901.4394*
 Howell, S. B., et al. 2003, *PASP*, 115, 1340
 Johnson, J. A., Winn, J. N., Cabrera, N. E., & Carter, J. A. 2009, *ApJ*, 692, L100
 Joshi, Y. C., et al. 2009, *MNRAS*, 392, 1532
 Jurić, M. & Tremaine, S. 2008, *ApJ*, 686, 603
 Lin, D. N. C., Bodenheimer, P., & Richardson, D. C. 1996, *Nature*, 380, 606
 Loeillet, B., et al. 2008, *A&A*, 481, 529
 Lubow, S. H. & Ogilvie, G. I. 2001, *ApJ*, 560, 997
 Madhusudhan, N. & Winn, J. N. 2008, *arXiv:807.4570*, 807
 Mandel, K. & Agol, E. 2002, *ApJ*, 580, L171
 Marcy, G., et al. 2005, *Progress of Theoretical Physics Supplement*, 158, 24
 Marcy, G. W. & Butler, R. P. 1992, *PASP*, 104, 270
 McLaughlin, D. B. 1924, *ApJ*, 60, 22
 Moorhead, A. V. & Adams, F. C. 2008, *Icarus*, 193, 475
 Narita, N., et al. 2009, *ArXiv e-prints*
 Noguchi, K., et al. 2002, *PASJ*, 54, 855
 Ohta, Y., Taruya, A., & Suto, Y. 2005, *ApJ*, 622, 1118
 Pont, F., et al. 2009, *ArXiv e-prints*
 Pont, F., Zucker, S., & Queloz, D. 2006, *MNRAS*, 373, 231
 Queloz, D., et al. 2000, *A&A*, 359, L13
 Rossiter, R. A. 1924, *ApJ*, 60, 15
 Tegmark, M., et al. 2004, *Phys. Rev. D*, 69, 103501
 Tonry, J., Burke, B. E., & Schechter, P. L. 1997, *PASP*, 109, 1154
 Tonry, J. L., et al. 2005, *PASP*, 117, 281
 Valenti, J. A. & Fischer, D. A. 2005, *ApJS*, 159, 141
 Winn, J. N., et al. 2009, *arxiv:0902.3461*
 Winn, J. N., et al. 2007, *ApJ*, 665, L167
 Winn, J. N., et al. 2005, *ApJ*, 631, 1215
 Wright, J. T., et al. 2009, *ApJ*, 693, 1084
 Wu, Y., Murray, N. W., & Ramsahai, J. M. 2007, *ApJ*, 670, 820

TABLE 1
RADIAL VELOCITY MEASUREMENTS OF WASP-14

Heliocentric Julian Date (HJD)	RV (m s ⁻¹)	Uncertainty (m s ⁻¹)	Telescope ^a
2454667.80421	-139.4	1.0	K
2454672.81824	-1008.4	1.3	K
2454673.83349	955.3	1.3	K
2454999.76227	151.6	6.3	S
2454999.76665	138.8	5.2	S
2454999.77091	133.6	5.9	S
2454999.77517	112.0	5.4	S
2454999.77943	110.2	5.5	S
2454999.79290	97.9	5.8	S
2454999.79716	89.8	5.4	S
2454999.80142	67.8	7.1	S
2454999.80600	65.8	6.0	S
2454999.81026	54.3	5.4	S
2454999.81452	49.0	5.2	S
2454999.81878	34.6	5.3	S
2454999.82901	4.9	4.7	S
2454999.83327	-6.9	4.5	S
2454999.84471	-38.3	5.4	S
2454999.84898	-46.0	4.8	S
2454999.85771	-70.3	4.9	S
2454999.86197	-76.8	5.1	S
2454999.86623	-92.5	4.7	S
2454999.87049	-111.3	4.5	S
2454999.87477	-114.5	5.7	S
2454999.87904	-124.9	6.0	S
2454999.88330	-131.0	5.8	S
2454999.88757	-148.0	5.5	S
2454999.89183	-161.0	6.0	S
2454999.89610	-154.8	5.6	S
2454999.90037	-175.6	5.8	S
2454999.90464	-187.6	5.4	S
2454999.90890	-190.4	6.7	S
2454999.91317	-215.8	7.1	S
2454999.92129	-228.0	8.0	S
2454999.96315	-330.4	8.8	S
2454999.96743	-331.1	7.8	S
2454999.97170	-350.1	9.2	S
2454999.98117	-372.5	5.6	S
2454999.98891	-378.0	5.4	S
2454999.99665	-398.5	5.9	S
2455000.00825	-416.6	5.7	S
2455000.01598	-429.6	6.4	S
2455014.86287	965.8	1.4	K
2455015.91393	-812.7	1.7	K

^a K: HIRES, Keck I 10m telescope, Mauna Kea, Hawaii. S: HDS, Subaru 8m telescope, Mauna Kea, Hawaii.

TABLE 2
RELATIVE PHOTOMETRY FOR WASP-14

Heliocentric Julian Date (HJD)	Relative Flux
2454963.85021	1.00064
2454963.85113	1.00127
2454963.85204	1.00024
2454963.85296	1.00086
2454963.85387	1.00115
2454963.85478	0.99986
2454963.85569	1.00183
2454963.85660	1.00005
...	...

NOTE. — The full version of this table is available in the online edition, or by request to the authors.

TABLE 3
SYSTEM PARAMETERS OF WASP-14

Parameter	Value
<i>Orbital Parameters</i>	
Orbital period, P [days]	2.2437704 ± 0.0000028
Mid-transit time, T_t [HJD]	$2454963.93676 \pm 0.00025$
Velocity semiamplitude, K_* [m s $^{-1}$]	989.9 ± 2.1
Argument of pericenter, ω [degrees]	253.10 ± 0.80
Orbital eccentricity, e	0.0903 ± 0.0027
Velocity offset, γ_{FIES} [m s $^{-1}$]	-4989.5 ± 3.4
Velocity offset, γ_{SOPHIE} [m s $^{-1}$]	-4990.1 ± 3.0
Velocity offset, γ_{HIRES} [m s $^{-1}$]	107.1 ± 2.1
Velocity offset, γ_{HDS} [m s $^{-1}$]	7.7 ± 2.5
<i>Spin-orbit Parameters</i>	
Projected spin-orbit angle λ [degrees]	$-33.1^\circ \pm 7.4^\circ$
Projected stellar rotation rate $v \sin i_*$ [km s $^{-1}$]	2.80 ± 0.57